


# The transcription factor RUNX2 fuels YAP1 signaling and gastric cancer tumorigenesis

Zhengjun Guo<sup>1</sup> | Kai Zhou<sup>2</sup> | Qiang Wang<sup>3</sup> | Yusheng Huang<sup>1</sup> | Jia Ji<sup>4</sup> | Yuan Peng<sup>1</sup> | Xiaoyue Zhang<sup>1</sup> | Taihao Zheng<sup>5</sup> | Zhen Zhang<sup>6</sup> | Daochen Chong<sup>3</sup> | Zhenzhou Yang<sup>1</sup> 

<sup>1</sup>Department of Cancer Center, The Second Affiliated Hospital of Chongqing Medical University, Chongqing, China

<sup>2</sup>Department of General Surgery and Center of Minimal Invasive Gastrointestinal Surgery, Southwest Hospital, Third Military Medical University (Army Medical University), Chongqing, China

<sup>3</sup>Pathology Department, Navy 971 Hospital of PLA, Qindao, China

<sup>4</sup>Department of Neurosurgery, Chongqing University Cancer Hospital, Chongqing, China

<sup>5</sup>Department of Oncology, Yongchuan Hospital of Chongqing Medical University, Chongqing, China

<sup>6</sup>Department of Plastic and Aesthetic Surgery, Southwest Hospital, Third Military Medical University (Army Medical University), Chongqing, China

## Correspondence

Zhenzhou Yang and Zhengjun Guo, Department of Cancer Center, The Second Affiliated Hospital of Chongqing Medical University, Chongqing, China.

Email: yangzz@cqmu.edu.cn (Z. Y.); gzhjx@126.com (Z. G.)

## Funding information

National Natural Science Foundation of China, Grant/Award Number: 81972793, 81972851 and 82002448; Chongqing Postdoctoral Science Foundation, Grant/Award Number: cstc2019jcyj-bshX0056

## Abstract

Despite considerable efforts in the detection and treatment of gastric cancer (GC), the underlying mechanism of the progression of GC remains unknown. Our previous work has demonstrated the remarkable role of Runx2-related transcription factor 2 (RUNX2), in fueling the invasion and metastasis of GC. The present study aimed to elucidate the role of RUNX2 in tumorigenesis of GC. We assessed Runx2 expression and its clinical significance via bioinformatic analysis of the Cancer Genome Atlas and Gene Expression Omnibus databases. Roles for Runx2 in self-renewal and tumorigenesis were examined *in vitro* and *in vivo*. Further bioinformatic analysis was applied to study the mechanism of GC progression. We found that Runx2 was highly expressed in the early stage of GC and positively correlated with a poor clinical outcome of patients. Runx2 was also significantly correlated with clinicopathological features, such as *Hp* infection, new neoplastic events, primary therapeutic outcome, ethnicity, race, and tumor stage. Multivariate analysis revealed that together with Runx2, age, cancer status, M stage, and T stage were independent prognostic factors for the outcome of GC patients. RUNX2 overexpression induced increased anchorage-independent colony formation, sphere formation, and tumorigenesis in GC cells *in vitro* and *in vivo*. Mechanistically, bioinformatic analysis indicated that yes1 associated transcriptional regulator (YAP1) might be a downstream target of RUNX2. Specific knockdown of YAP1 reduced the tumor-initiating ability of GC cells induced by ectopic Runx2 expression. Our findings support the hypothesis that RUNX2 exerts oncogenic properties via YAP1 regulation, highlighting essential roles for RUNX2 and YAP1 in gastric carcinogenesis and suggesting potential therapeutic targets.

## KEYWORDS

gastric cancer, Hippo, RUNX2, tumorigenesis, YAP1

This is an open access article under the terms of the Creative Commons Attribution-NonCommercial License, which permits use, distribution and reproduction in any medium, provided the original work is properly cited and is not used for commercial purposes.

© 2021 The Authors. *Cancer Science* published by John Wiley & Sons Australia, Ltd on behalf of Japanese Cancer Association.

## 1 | INTRODUCTION

Gastric cancer (GC) is the second leading cause of cancer-related mortality worldwide, especially in Eastern Asian countries.<sup>1</sup> Almost 990,000 new cases are diagnosed worldwide every year.<sup>2</sup> GC is also the main contributor to the world burden of disability-adjusted life-years from cancer worldwide.<sup>2</sup> One contributing reason is the tumorigenesis potential of GC cells.<sup>3</sup> Thus, it is of great importance to explore novel biomarkers and therapeutic targets for GC.

Runx-related transcription factor 2 (RUNX2), a versatile transcription factor in osteoblast differentiation, also serves as a scaffold for tumorigenesis and cancer progression.<sup>4</sup> Our previous work revealed that RUNX2 was seriously involved in GC invasion and metastasis.<sup>5</sup> However, the critical roles of RUNX2 in GC tumorigenesis cells are largely unknown.

In this study, we explored the role of RUNX2 in GC self-renewal potential and tumorigenesis, as well as its clinical significance for GC patients. By mining datasets from the Cancer Genome Atlas (TCGA) and the Gene Expression Omnibus (GEO), we found a close relationship between RUNX2 and clinicopathological features. We demonstrated that RUNX2 showed a crucial function in modulating the self-renewal and tumorigenesis abilities of GC cells in mouse xenograft models. Our findings provide new evidence that RUNX2 is a valuable indicator for the detection of early-stage GC, a predictor of the outcome of GC patients, and a potential treatment target for GC prevention.

## 2 | MATERIALS AND METHODS

### 2.1 | Data mining of public databases

GC samples from publicly available datasets from the TCGA and GEO databases were enrolled. The TCGA GC (stomach adenocarcinoma, STAD) gene expression dataset can be acquired from <https://genome-cancer.ucsc.edu/proj/site/hgHeatmap/?datasetSearch=STAD>. STAD data and microarray data were processed with the NetworkAnalyst webtool.<sup>6,7</sup> Correlations between clinical features and gene expression were evaluated with MEXPRESS.<sup>8</sup>

GC datasets of the GEO database were explored via the Kaplan-Meier (K-M) Plotter database.<sup>9</sup> Data batch normalization and processing were performed with R software (version 3.5.3) with a Bioconductor package. Quality control was performed and biased arrays were excluded according to the approach.<sup>10</sup>

### 2.2 | Animals and xenografts

Five-week-old male nude mice with a BALB/c-nu background were purchased from the Laboratory Animal Center of Southwest Hospital (Chongqing, China). Different groups of GC cells were subcutaneously injected into the mice. Eight weeks after tumor implantation, all mice were sacrificed and the xenografts were harvested.

The weight of xenografts was carefully detected and recorded for statistical analysis. Tissue samples were fixed, paraffin-embedded, and sectioned into 5- $\mu$ m slices for Gill's hematoxylin and eosin (H&E) staining. All animal studies were carried out following the regulations of the Administration of Affairs Concerning Experimental Animals (China, 1988) and approved by the Animal Care and Use Committee of Southwest Hospital.

### 2.3 | Cell lines and cell culture

The human GC cell line MGC803 was obtained from the Cell Bank of Shanghai Institute of Cell Biology (Chinese Academy of Sciences). The human primary GC cell line XN0422 (diffuse-type by Lauren classification) was provided by the Institute of Pathology and Southwest Cancer Center, Army Medical University, Chongqing, China, as described previously.<sup>11</sup> The construction of stable RUNX2 overexpression and knockdown gastric cancer cell lines were described previously.<sup>5</sup> For yes1 associated transcriptional regulator (YAP1) knockdown in MGC803-exRUNX2 cells, two pairs of shRNAs were synthesized and cloned into a pMAGic 7.1 lentiviral vector. The sequences of shRNAs of YAP1 have already been certificated by Li Jipeng's team.<sup>12</sup> All cells were cultured in RPMI 1640 medium (Gibco, Invitrogen) supplemented with 10% fetal bovine serum (FBS, HyClone, Thermo Scientific), 100 U/ml penicillin, and 100  $\mu$ g/ml streptomycin at 37°C in 5% CO<sub>2</sub>. The cells were harvested for experiments after they reached 70%-80% confluence.

### 2.4 | RNA extraction and qRT-PCR

Total RNA from GC cells was isolated using TRIzol (Takara) according to the manufacturer's specifications. Then, quantitative real-time PCR (qRT-PCR) was performed to detect mRNAs. In brief, 0.2  $\mu$ g of total RNA extracted from cells was reverse transcribed to cDNA using the RevertAid First Strand cDNA Synthesis Kit (Fermentas) and amplified with PCR amplification primers in a DreamTaq™ Green PCR Master Mix system (Fermentas). All primer sequences are shown in Table S1. qRT-PCR was performed with SYBR Green mix (Fermentas) and detected by the CFX96 system (BioRad). RNase-free water was used as a blank control. The qRT-PCR was performed in triplicate.

### 2.5 | Western blotting

Western blotting (WB) was performed as described previously. In brief, cells were harvested and washed twice with ice-cold PBS and lysed on ice with protein extraction reagent (Pierce) supplemented with 1% protease inhibitor (Pierce). The lysed samples were then centrifuged at 14,000 $\times$  g (4°C for 20 minutes), and the protein concentrations were detected with a bicinchoninic acid (BCA) protein assay kit (Pierce). Total protein was denatured, separated by SDS-PAGE and then transferred

to PVDF membranes (Millipore). The membranes were then incubated at 4°C overnight with the following antibodies: mouse anti-RUNX2 (Sigma-Aldrich), rabbit anti-GAPDH (Cell Signaling Technology), mouse anti-TAZ (Abnova), rabbit anti-p-YAP1 (Cell Signaling Technology) or mouse anti-YAP1 (Abnova). Then, the membranes were incubated for 1 hour with peroxidase-conjugated secondary antibody (Beyotime). The bands were detected by chemiluminescence using SuperSignal West Femto Maximum Sensitivity Substrate (ECL, Pierce-Thermo Scientific). The blots were then stripped and reprobbed with an anti- $\beta$ -actin monoclonal antibody (Sigma).

## 2.6 | Colony formation assay and limiting dilution assay

Cell colony formation assays and limiting dilution assays were performed to test the self-renewal ability of GC cells *in vitro*. Equal amounts of MGC803-Control and MGC803-exRUNX2 or XN0422-mock and XN0422-shRUNX2 cells were seeded into a six-well plate and cultured for 2 weeks. The colonies that formed were carefully fixed with 4% formaldehyde for 20 minutes and stained with 1% crystal violet. The number of colonies was counted and statistically analyzed. Different concentrations of cells (0, 2, 5, 10, and 20) were seeded into 96-well plates and cultured in conditioned culture medium for 2 weeks. The number of spheres formed was calculated and recorded. A linear regression model was applied to compare the slope of each group.

## 2.7 | Immunohistochemistry

Consecutive gastric tissue (mucosal dysplasia and early-stage GC) sections (4  $\mu$ m) were mounted on salinized slides. Tissue sections were deparaffinized and rehydrated in graded ethanol. Hydrogen peroxide (3%) was applied for 30 minutes at 37°C to quench endogenous peroxidase. The sections were washed three times with PBS. RUNX2 antigen was retrieved using citrate buffer (pH 6.0) by heating for 2 minutes in a Pascal pressure chamber (DAKO). Slides were then incubated with mouse anti-RUNX2 (CST, USA) at 4°C overnight. After washing the primary antibody away with PBS, HRP-conjugated secondary antibody (Dako) was added to the membranes and incubated for 40 minutes at 37°C. After washing with PBS, diluted 3,3'-diaminobenzidine (DAB) (Dako) was added. The RUNX2 immunohistochemical staining in the tissue samples was classified into four categories based on the intensity (score of 0 to 3) according to the reported method.<sup>13</sup> Ki67 index was assessed according to the recommendations from the International Ki67 in Breast Cancer working group.<sup>14</sup> All slides were evaluated independently by two pathologists in a blinded manner.

## 2.8 | Flow cytometric analysis

The Aldehyde Dehydrogenase (ALDH) activity of GC cells was detected according to the manufacturer's instructions of the Aldefluor

kit (Stem Cell Technologies). Briefly, GC cells were suspended in Aldefluor buffer containing ALDH substrate and incubated for 45 minutes at 37°C. For flow cytometric sorting, cell samples were sorted with a FACSAria II (BD Bioscience).

## 2.9 | Statistical analysis

All experiments were performed at least three times, and the results are reported as the means  $\pm$  SDs. Statistical analysis was performed using Student's *t* test with SPSS software (LEAD Technologies). The K-M method and log-rank test were used to test the overall survival (OS) of GC patients. The Cox proportional hazards regression model was used for multivariate analysis of the combined contribution of RUNX2 and clinicopathological features to the OS or prognosis of patients. Principal component analysis (PCA) was performed on the RUNX2<sup>low</sup> and RUNX2<sup>high</sup> cases from the TCGA database. Each principal component is a linear combination of optimally weighted original variables, thus it is often possible to ascribe meaning to the components. All data were analyzed using GraphPad Prism 8.0 or SPSS 20.0. Differences with *P* < .05 were considered statistically significant.

## 3 | RESULTS

### 3.1 | Elevated Runx2 expression predicts a poor clinical outcome in GC patients

Previously, an interesting finding<sup>5</sup> proved that Runx2 was highly detected in tissues of early-stage GC compared with gastric mucosa dysplasia tissues (*P* < .01; Figure 1A). Immunohistochemical staining of RUNX2 also showed that it stains higher in early-stage GC tissues (Figure 1B, right) than in gastric mucosa dysplasia tissues (Figure 1B, left), which might be a clue for the contribution of Runx2 to gastric carcinogenesis. To further validate this relationship, we mined the datasets from the TCGA and GEO databases. A cohort of 376 GC patients with Runx2 expression was obtained from TCGA. Bioinformatics analysis based on the datasets revealed higher Runx2 expression in cancer tissues than in normal tissues (*P* = .007; Figure 1C). By mining the TCGA dataset with MEXPRESS,<sup>8</sup> we found that Runx2 expression was significantly correlated with Hp infection (*P* = .037), new neoplastic event type (*P* = .032), primary therapeutic outcomes success (*P* = .034), ethnicity (*P* = .021), race (*P* = .008), and tumor stage (*P* = .014) (Figure 1D). Furthermore, K-M survival analyses revealed that GC patients with high Runx2 expression showed a much shorter OS time and cancer-free survival (CFS) time than patients with low Runx2 expression (*P* = .024 and *P* = .046, respectively; Figure 1E,F). Moreover, a batch of cohorts with 876 GC patients from the GEO was analyzed for the clinical significance of Runx2 expression. Similarly, higher Runx2 expression was significantly associated with poor OS time and CFS time in GC patients (*P* < .001 for both OS and CFS; Figure 1G,H). Multivariate

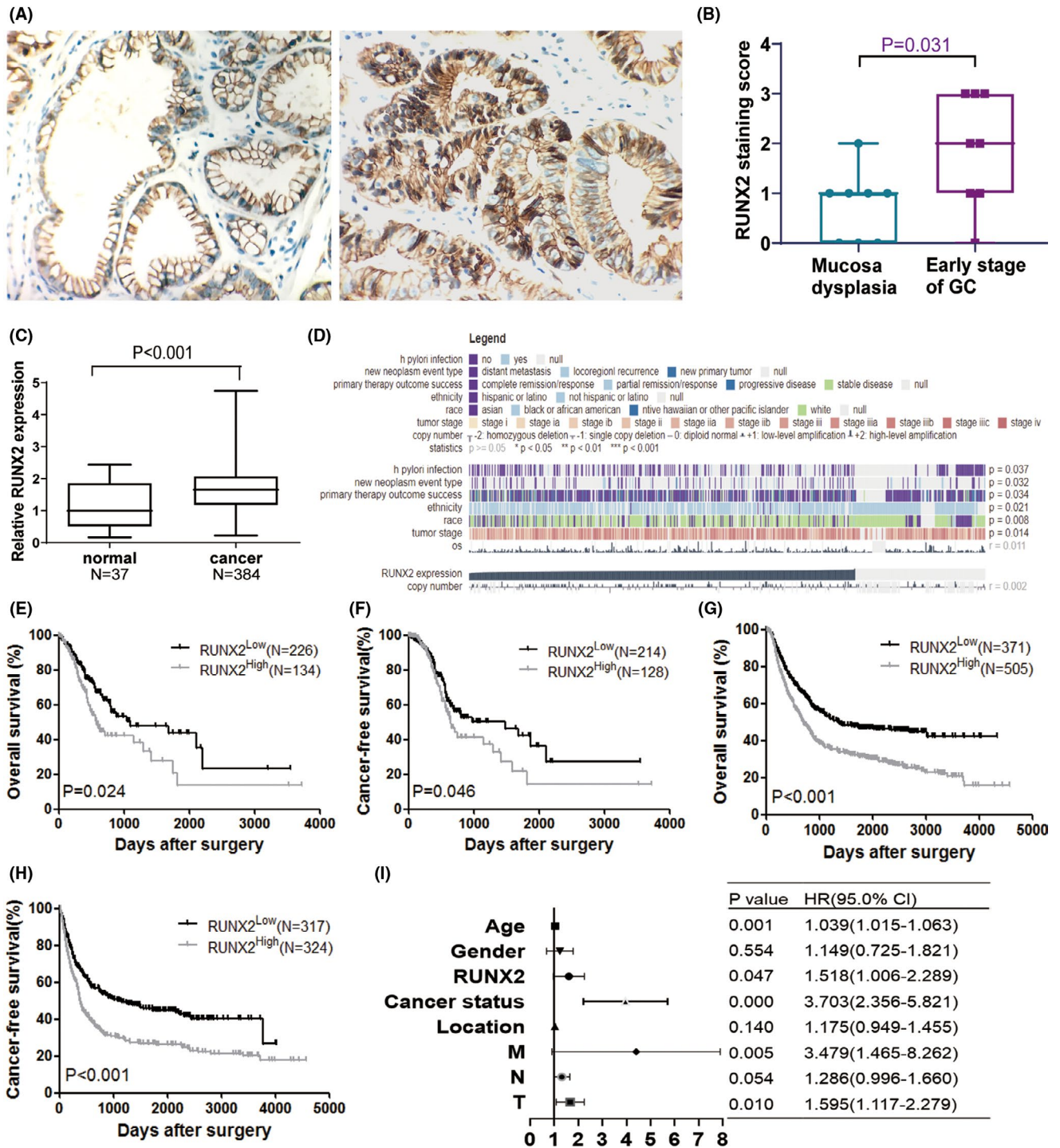


**FIGURE 1** Clinical significance of Runx2 in gastric cancer (GC). A, Representative images of RUNX2 staining in mucosa dysplasia tissues and early stage GC tissues by immunohistochemistry. The left image is mucosal dysplasia tissue and the right image is early-stage GC tissue. RUNX2 immunohistochemical staining in the tissue samples was classified into four categories according to the intensity (score of 0 to 3). B, Comparison of the staining score of RUNX2 in mucosa dysplasia tissues and early stage of GC tissues. C, Runx2 mRNA expression in GC tissues and in normal tissues in the Cancer Genome Atlas (TCGA) stomach adenocarcinoma cohort. D, Correlation analysis of Runx2 with clinical features, such as Helicobacter pylori (Hp) infection, new neoplasm event type, primary therapy outcome, ethnicity, race, and tumor stage by MEXPRESS analysis. E, Kaplan-Meier (K-M) curve for overall survival of patients stratified by Runx2 expression level from the TCGA cohort. F, K-M curve of cancer-free survival (CFS) in GC patients with high or low Runx2 expression from the TCGA cohort. G, K-M curve for overall survival of GC patients with different Runx2 expression from the Gene Expression Omnibus (GEO) cohort. H, K-M curve for the CFS of patients stratified by Runx2 expression level from the GEO cohort. I, Multivariate analysis was performed using a Cox proportional hazards regression model and the results are shown in a forest plot.

analysis with a forest plot was applied to determine the significance of Runx2 when considering the clinicopathological features in GC. The results revealed that Runx2, cancer status, age, and T and M status were significant clinical indicators of poor outcomes in GC patients (Figure 1I). These results suggest that RUNX2 might participate in the initiation step of gastric carcinogenesis and serve as a crucial factor for the prognosis of GC patients.

### 3.2 | Increased RUNX2 expression maintains the self-renewal ability of GCSCs in vitro

To investigate the potential role of RUNX2 in GC stem cells (GCSCs), we first assessed the expression of RUNX2 in GC cells. We enriched and isolated spheroid cells from the GC cell line MGC803 and the primary GC cell line XN0422 in conditioned serum-free culture medium and confirmed their stem cell-like properties. qRT-PCR demonstrated a higher level of Runx2 in the isolated GCSCs than in the monolayer cells (Figure 2A). Similar results were also observed by western blot analysis (Figure 2B) and immunofluorescence analysis (Figure 2C).

We next studied the effect of RUNX2 on the stemness of GC cells. We overexpressed RUNX2 in MGC803 cells and knocked down RUNX2 in XN0422 cells as described previously.<sup>5</sup> Colony formation assays demonstrated that RUNX2-overexpressing MGC803 cells showed a substantial increase in colony formation ability, while RUNX2 knockdown XN0422 cells showed impaired colony formation ability (Figure 2D,E). Sphere formation assays and limiting dilution assays were applied to evaluate the sphere-forming ability. The results indicated that RUNX2 overexpression increased the number of spheres formed compared with that in the control group ( $P < .05$ ; Figure 2F). Similar to the results of the colony formation assays, silencing RUNX2 decreased the number of spheres formed compared with that in mock cells ( $P < .01$ ; Figure 2G). These findings revealed that RUNX2 contributes to maintaining the self-renewal potential of GCs.

### 3.3 | RUNX2 contributes to the tumorigenesis of GC in vivo

We assessed the effect of RUNX2 on the tumorigenesis and progression of GC using a xenograft model. RUNX2-overexpressing MGC803 cells and control cells ( $5 \times 10^5$ ) were implanted subcutaneously into nude mice to create a xenograft model. No significance in tumor weight was observed between RUNX2-overexpressing MGC803 cells and the control group (Figure 3A,C). Additionally, RUNX2 expression was stably silenced in XN0422 cells; after inoculation of XN0422-shRUNX2 and mock cells into the flanks of nude mice, weight of the tumor derived from XN0422-shRUNX2 cells decreased significantly, as compared with the XN0422-mock cells (Figure 3B,C). As shown in Table S2, mice engrafted with RUNX2 knockdown XN0422 cells exhibited impaired tumorigenicity compared to XN0422-mock cell-engrafted mice. Further

immunohistochemical staining revealed a higher level of Ki67 staining in RUNX2-overexpressing xenografts than in control xenografts; the tumors derived from RUNX2-silenced XN0422 cells showed lower Ki67 staining than those derived from the mock cells (Figure 3D). Moreover, a higher Ki67 index was demonstrated in RUNX2-overexpressing xenografts than in control xenografts ( $P = .008$ ; Figure 3E), whereas a decreased Ki67 index was demonstrated in the xenografts from the RUNX2-silenced cells ( $P = .015$ ; Figure 3E). These data suggest that ectopic expression of RUNX2 fuels GC tumorigenesis. RUNX2 may therefore be a crucial modulator of cancer progression during the early stage of GC and in maintaining the malignant potential of GC cells.

### 3.4 | Functional analysis of DEGs associated with Runx2 in the TCGA dataset

According to the cutoff values, samples in the TCGA dataset were divided into two groups (RUNX2<sup>high</sup> and RUNX2<sup>low</sup> groups). After comparison, over 241 differentially expressed genes (DEGs) were detected ( $P < .05$ ,  $|\log_2FC| > 0.5$ ), among which 184 genes were positively correlated with Runx2 and 57 genes negatively correlated, as shown in the heatmap and volcano map (Figure 4A,B). Then, gene set enrichment analysis (GSEA) was performed to further understand the significantly activated signaling pathways in the RUNX2<sup>high</sup> group. The Hippo signaling pathway was significantly activated in this group (see the heatmap [Figure 4C] and GSEA map [ $P = .0017$ ,  $ES = 0.3633$ ; Figure 4D]). Linear regression analysis also revealed that the Runx2 and Yap1 expression levels were positively correlated ( $P = .011$ ; Figure 4E).

We reasoned that more comprehensive analysis of the TCGA dataset could help to unveil the molecular nature of GC. Therefore, PCA was performed based on the TCGA whole-genome dataset to evaluate the variance of principal components. The contribution rates of the top three components, PC1, PC2, and PC3, were 12.5%, 7.9%, and 5.3%, respectively (Figure S1A). The cumulative contribution rate of the first three components was only 25.7%. High (red ball) and low (blue ball) cases are shown in the score plot (each point represents a tumor sample; Figure S1A). A three-dimensional PCA loading plot showed that four clusters accounted for the majority of the variance (each point represents a gene; Figure S1B). T-distributed stochastic neighbor embedding (t-SNE), another machine learning algorithm for dimension descending, was also performed to evaluate the variance of the sample. Similar results were obtained by t-SNE, in that the two groups did not display a clear separation (Figure S1C). Furthermore, the DEGs involved in the process were also analyzed. Kyoto Encyclopedia of Genes and Genomes (KEGG) analysis and gene ontology (GO) analysis were performed to reveal the significantly activated signaling pathways and biological processes that were influenced by Runx2 in GC (Table S3). In summary, these bioinformatic results revealed that Hippo signaling was activated in GC cases with high Runx2 levels. Yap1 and Taz have been reported to be crucial modulators of the Hippo signaling pathway that maintain the self-renewal potential of GC cells.<sup>15</sup> Taken together, these findings

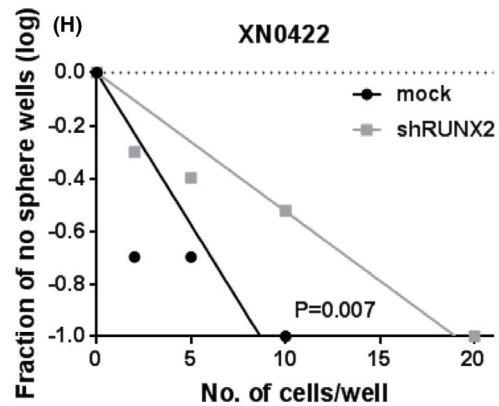
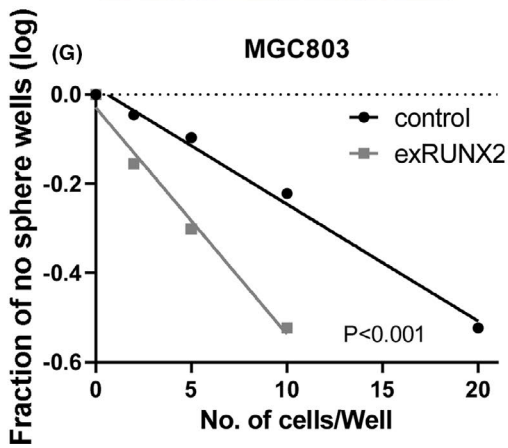
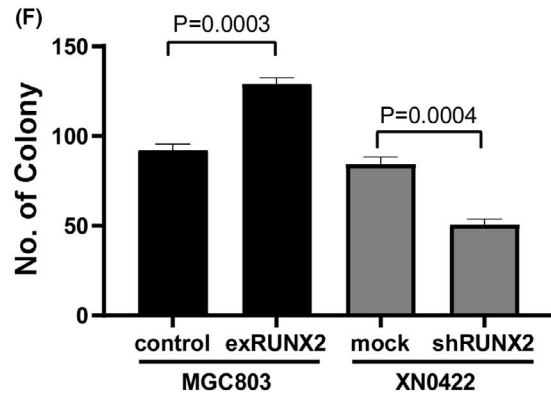
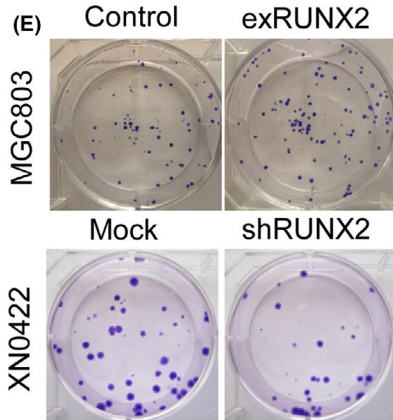
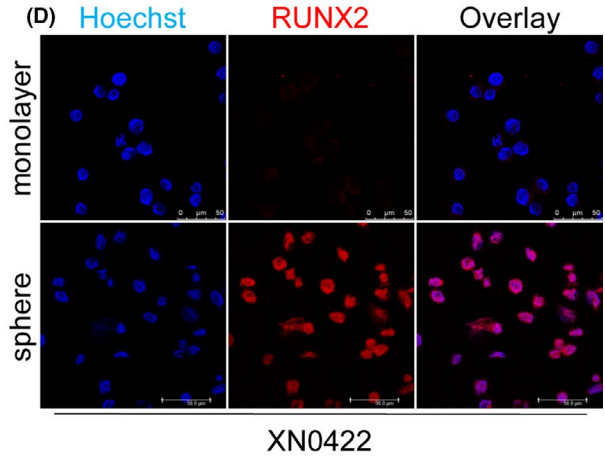
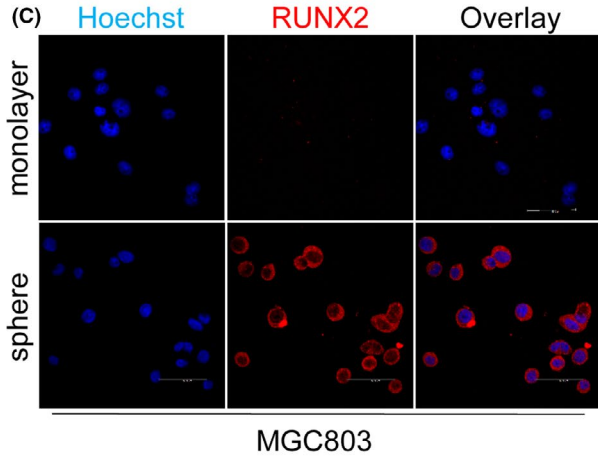
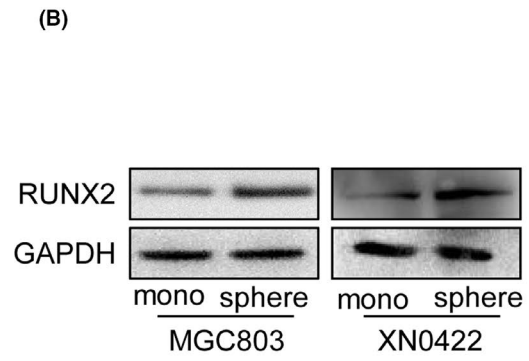
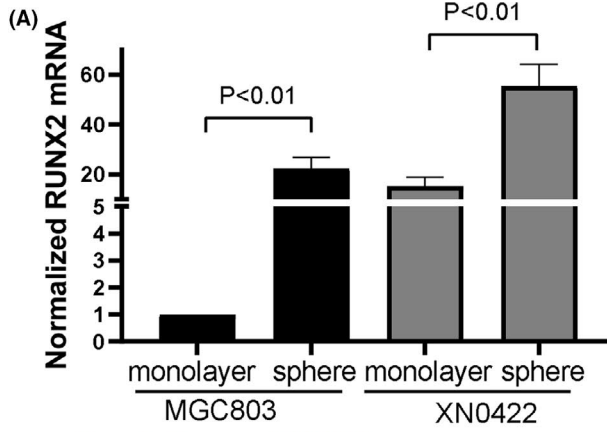
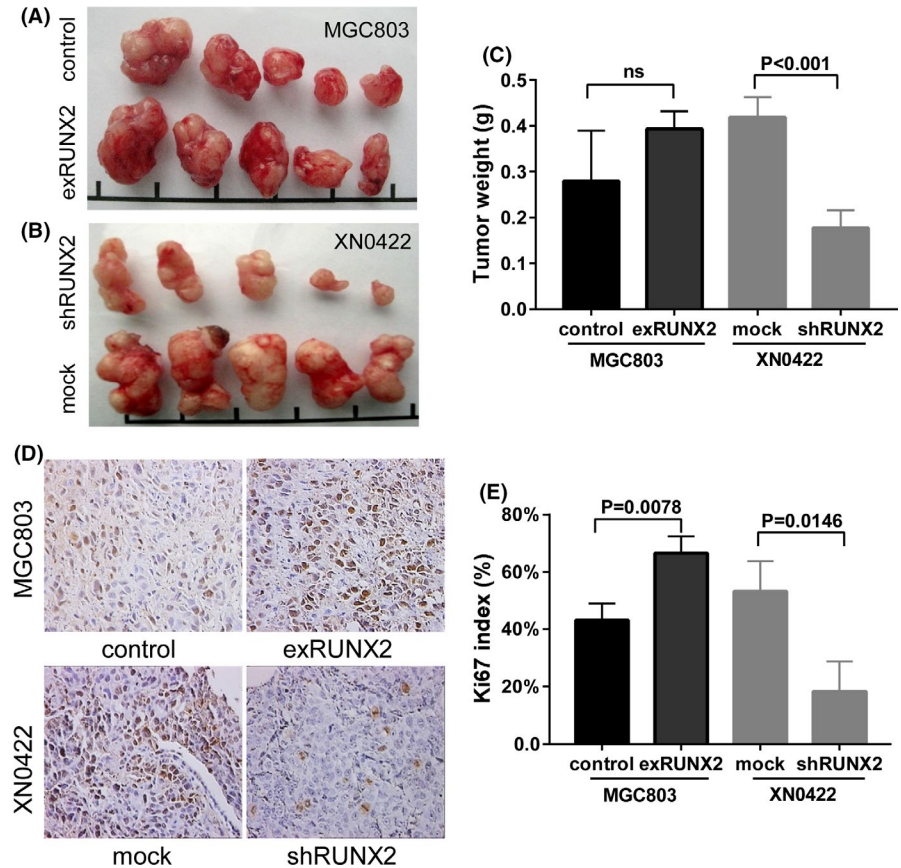


**FIGURE 2** RUNX2 is highly expressed in gastric cancer (GC) stem cells and maintains their self-renewal ability. A and B, Levels of RUNX2 were confirmed at the mRNA and protein level in monolayer cells and spheroid cells of MGC803 and XN0422 by real-time PCR and Western blotting. C and D, Immunofluorescence staining of RUNX2 (red) in monolayer cells and spheroid cells of MGC803 and XN0422. Nuclei were counterstained with Hoechst (blue). Scale bar = 50  $\mu$ m. E, Representative images of the colony formation assays showed the colony formation ability in overexpression experiments and in knockdown experiments. F, Statistical analysis of overexpression experiments (MGC803-control vs MGC803-exRUNX2) and knockdown experiments (XN0422-mock vs XN0422-shRUNX2). G, Limiting dilution assay was undertaken to compare the sphere formation potential of MGC803-control and MGC803-exRUNX2. H, Limiting dilution assay was performed to assess the sphere formation ability of XN0422-mock and XN0422-shRUNX2. Error bars represents for SD. All data shown are representative of three independent experiments

**FIGURE 3** RUNX2 enhances the tumorigenesis of gastric cancer (GC) cells in a xenograft mouse model. A, Images of xenografts in nude mice. The upper panel is xenografts formed by MGC803 and the lower panel is xenografts formed by XN0422. C, The weights of xenografts in the MGC803-control group vs RUNX2-overexpressed group and XN0422-mock group vs XN0422-shRUNX2 group. Five samples for each group. D, Ki67 index in xenografts from the MGC803 and XN0422 groups. E, The Ki67 index was statistically analyzed. Five high-power fields per sample were selected for Ki67 index assessment. Error bars represents for SD.



suggest that Hippo signaling might participate in RUNX2-induced GC tumorigenesis and progression.

### 3.5 | Molecular signatures regulated by RUNX2 in GC

To understand the molecular complexity, identify the downstream targets, and determine the associated biological functions of RUNX2 in GC, RUNX2 was silenced in XN0422 cells. After pairwise comparison based on the microarray results, 97 DEGs were obtained and are illustrated in the volcano map and heatmap (Figure 5A,B). Furthermore, KEGG and GO analyses were performed, and the top 10 significantly enriched signaling pathways, biological processes (BPs), molecular functions (MFs), and cellular components (CCs) were revealed (Figure 5C,D). For KEGG analysis, 37 significantly enriched pathways were determined ( $P < .05$ ; Figure 5C and Table S4).

Detailed information about GO analyses (BP, MF, and CC) is shown in Table S5. The Hippo signaling pathway showed the highest enrichment score (ES = 0.6667; Figure 5C).

To illustrate crosstalk, a protein-protein interaction (PPI) network was constructed via NetworkAnalyst based on the Search Tool for the Retrieval of Interacting Genes/Proteins (innateDB) Interactome database.<sup>16</sup> According to the score of centrality degree and betweenness, significantly up/down-regulated hub genes were found (Table S5). The results revealed that HIF1A, SKP2, EPAS1, YAP1, SOCS3, SAT1 CXCR4, and RUNX2 were the top eight significantly up-regulated hub genes during tumorigenesis in RUNX2-overexpressing GC cells (Figure 6A).<sup>17</sup> Heatmap and GSEA analyses were performed, and the results showed that the Hippo signaling pathway was significantly activated (Figure 6B,C). These bioinformatic results indicated that YAP1 and HIPPO signaling may be downstream of RUNX2 in GC. Furthermore, we verified the results in GC cells via RT-PCR and WB. The results revealed that ectopic expression of RUNX2 in

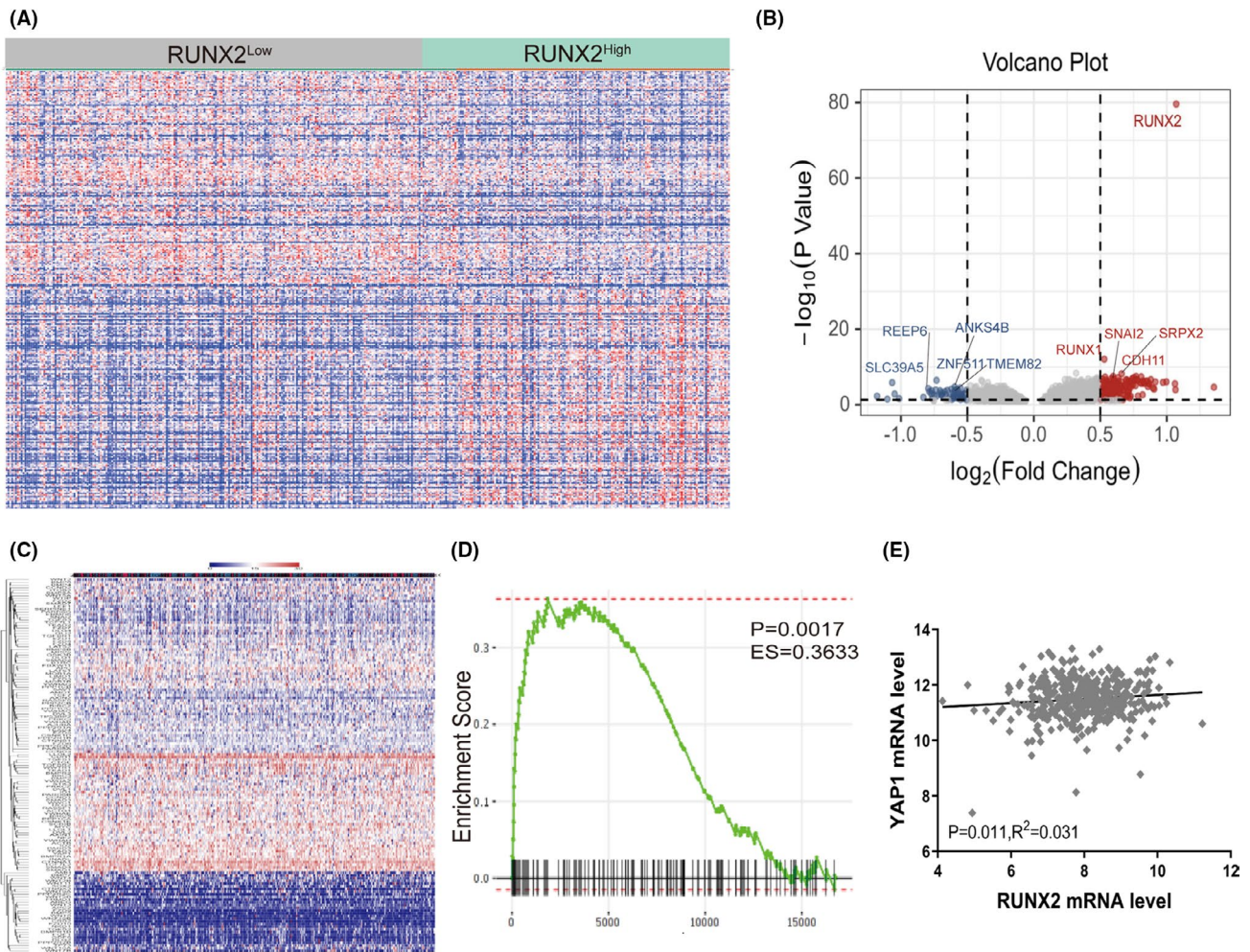


**FIGURE 4** Bioinformatic analysis of gastric cancer (GC) data from the Cancer Genome Atlas (TCGA) database. A, Heatmap of significantly differentially expressed mRNAs between Runx2<sup>high</sup> and Runx2<sup>low</sup> samples from the TCGA database. B, Volcano map of differentially expressed mRNAs. Red and blue spots represent significantly up-regulated and down-regulated genes, respectively. Top five up/down-regulated genes are listed. C, Heatmap of significantly enriched genes in the Hippo signaling pathway from the TCGA database. D, Gene set enrichment analysis profile of the Hippo signaling pathway in the TCGA database stratified by Runx2 level. E, The linear correlation between Runx2 and Yap1 was analyzed by Spearman's rank correlation coefficient

MGC803 cells induced elevated Yap1 expression, while silencing RUNX2 in XN0422 reduced the mRNA expression of Yap1 ( $P < .01$  for both groups; Figure 6D). The protein levels of YAP1 and p-YAP1 were also detected by WB. The results revealed that YAP1 might be in a same trend with RUNX2, while the p-YAP1 was not affected by RUNX2 in MGC803 cells and declined in XN0422-shRUNX2 cells (Figure 6E). These results indicate that YAP1 might be a downstream target of RUNX2 in gastric carcinogenesis.

### 3.6 | YAP1 blockade alleviates the tumor-initiating ability of GC cells induced by RUNX2 expression

To further verify the correlation between YAP1 and RUNX2, the expression of YAP1 was silenced in MGC803-exRUNX2 cells. We compared the tumorigenic potential of MGC803-exRUNX2 cells with or without YAP1 silencing in immunodeficient nude mice. As shown

in Figure 7A, xenografts derived from MGC803-exRUNX2-shYAP1 cells were significantly smaller than those derived from MGC803-exRUNX2-Scramble cells (Figure 7A). Additionally, the weight of xenografts from MGC803-exRUNX2-shYAP1 cells was lower than that of xenografts from the other groups ( $P = .0019$ ; Figure 7B). ALDH is considered a tumor stem cell marker in GC. We therefore assessed the level of ALDH in GC to verify the tumorigenic potential. The results revealed that after silencing YAP1 in MGC803-exRUNX2 cells, the ALDH expression rate sharply declined from 28.6% to 12.8% (Figure 7C). These results indicate that YAP1 is a key downstream regulator of RUNX2 in the process of GC initiation.

## 4 | DISCUSSION

GC is one of the leading causes of cancer-related death worldwide, especially in China. The majority of GC cases are diagnosed



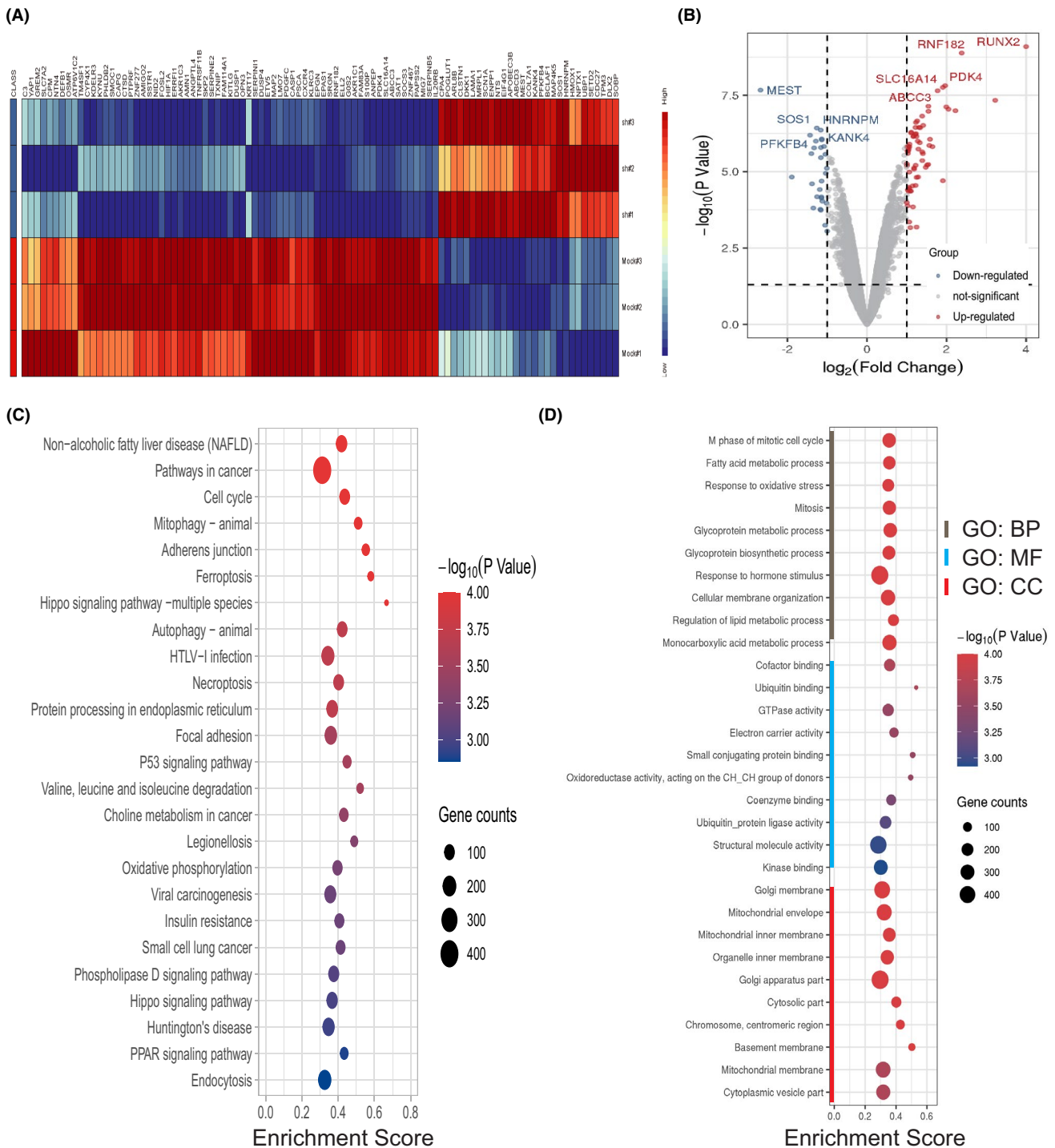


**FIGURE 5** Bioinformatic analysis of gastric cancer microarray data. A, Heatmap of differentially expressed mRNAs between XN0422-mock and XN0422-shRUNX2 cells. B, Volcano map of differentially expressed genes. Red and blue spots represent significantly up-regulated and down-regulated genes, respectively. Top five up/down-regulated genes are listed. C, Kyoto Encyclopedia of Genes and Genomes (KEGG) pathway enrichment analyses for the significant differentially expressed genes. D, Top 10 enriched Gene Ontology (GO) biological process (BP), molecular function (MF) and cellular component (CC) terms are listed

at an advanced stage, when the treatment approaches are limited and the prognosis is poor. However, early diagnosis allows the opportunity for effective treatment options and means a better outcome for GC patients. It has been postulated that a rare subpopulation of cancer cells, known as cancer stem-like

cells (CSCs), has strong tumorigenic capacity and is responsible for maintaining malignant potential.<sup>18,19</sup> Here, we proved that RUNX2 is highly expressed in GCSCs, fuels the tumorigenesis of GC cells via the YAP1 signaling pathway, and predicts the prognosis of GC patients.

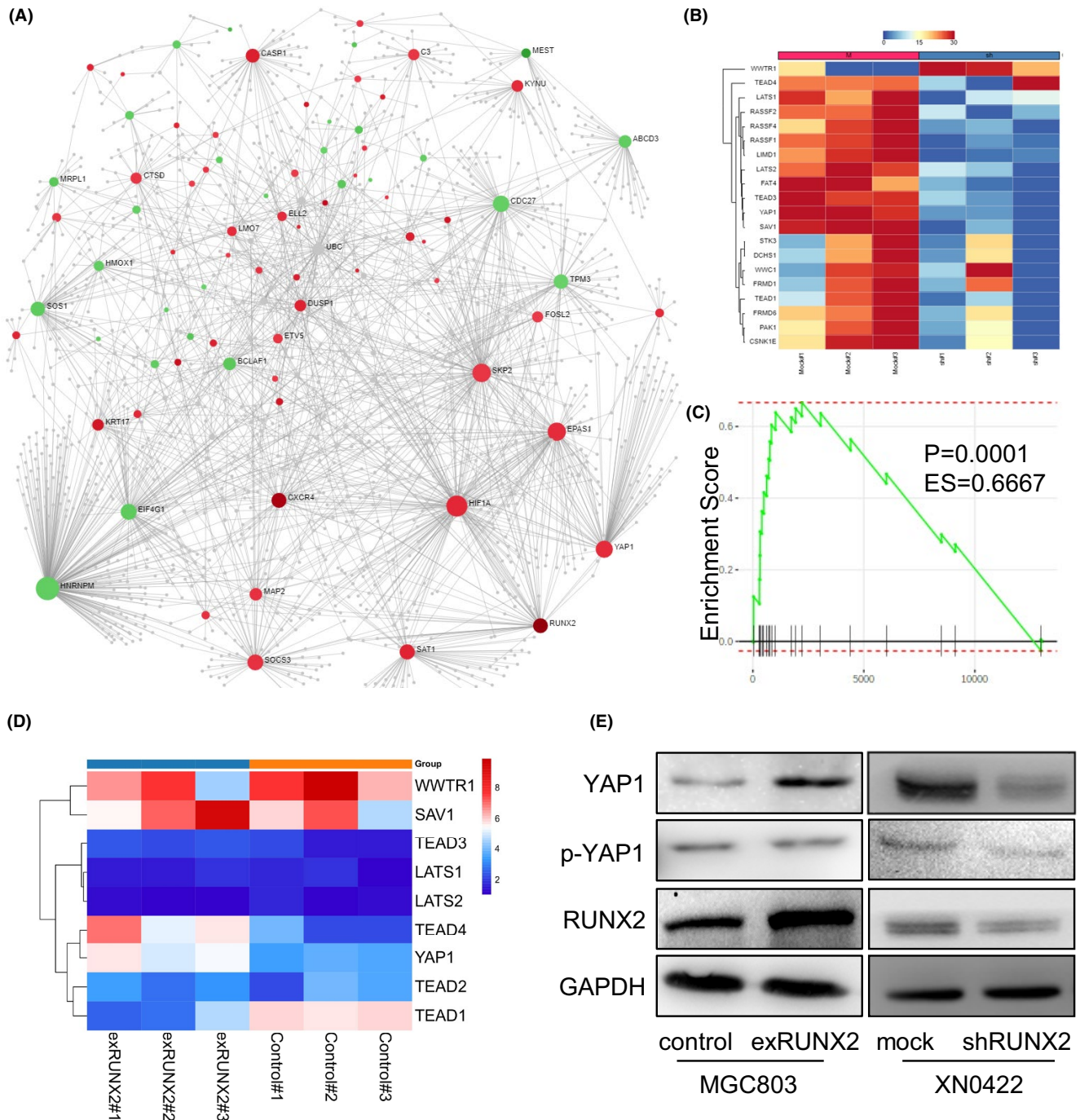
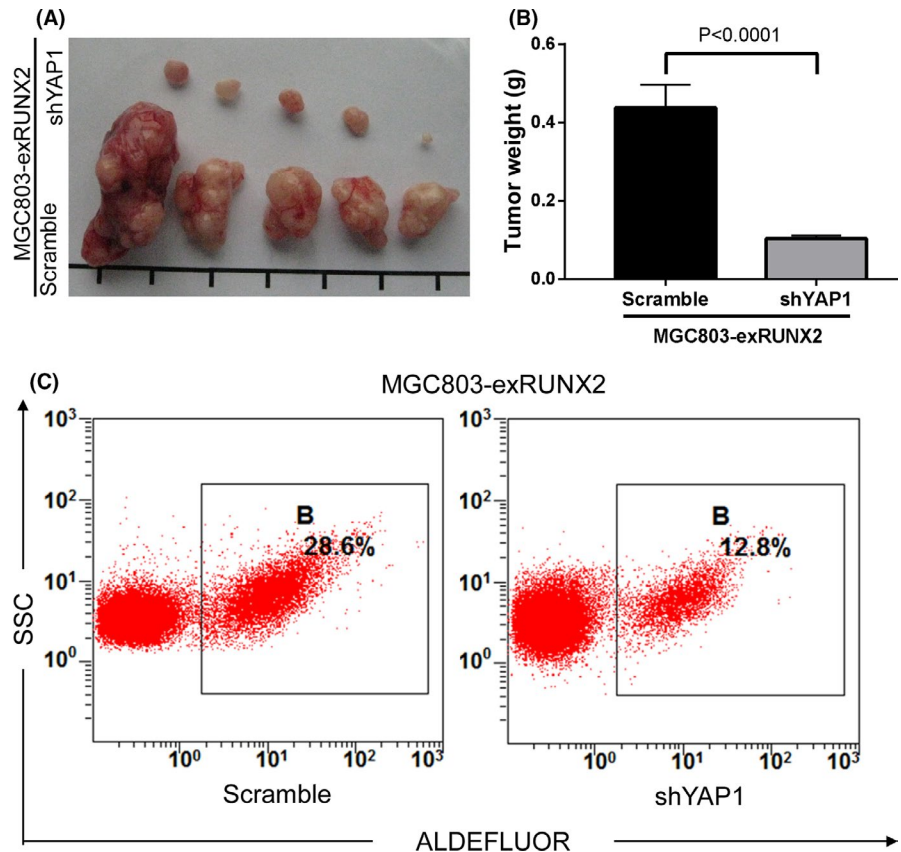


**FIGURE 6** YAP1 is a downstream target of RUNX2 in GC. A, The complete protein-protein interaction network of involved differentially expressed genes is shown. Red dots indicate up-regulated hub genes, green dots indicate down-regulated hub genes, and gray edges indicate the interactions between genes. The size of the dots represents the regulatory capacity, and larger dots indicate stronger regulatory capacity. B, Heatmap of genes associated with the Hippo signaling pathway. C, Gene set enrichment analysis of the Hippo signaling pathway. D, Heatmap presents the expression of Hippo signaling-related genes detected in MGC803 cells (control vs exRUNX2). Data are expressed as the means  $\pm$  SDs ( $n = 3$ ). E, Levels of RUNX2, YAP1, and p-YAP1 in MGC803 (control vs exRUNX2) and XN0422 cells (mock vs shRUNX2) were analyzed by Western blotting

Patients with GC are in dire need of effective therapeutic approaches. Accumulating evidence shows that GCSCs are responsible for the initiation of tumor formation and the maintenance of malignant potential.<sup>20</sup> Previously, our group proved that RUNX2 transcriptionally promotes the invasion and metastasis of GC cells via

CXCR4. Moreover, we found that RUNX2 is also highly expressed in GCSCs, therefore we sought to identify the role of RUNX2 in tumor initiation. Here, we demonstrated that RUNX2 serves as a potential diagnostic biomarker for GC patients and plays a central role in the maintenance of self-renewal potential in GC cells.

**FIGURE 7** YAP1 blockade impairs the tumor-initiating ability of gastric cancer (GC) cells induced by RUNX2 overexpression. A, Images of xenografts derived from the scramble group and shYAP1 group of MGC803-exRUNX2 cells. B, Tumor weights of MGC803-exRUNX2-Scramble and MGC803-exRUNX2-shYAP1 cells were statistically analyzed. C, Flow cytometric sorting of aldehyde dehydrogenase (ALDH)-positive cells from the MGC803-exRUNX2-Scramble and MGC803-exRUNX2-shYAP1 cells. Error bars represents for SD.



RUNX2, a member of the RUNX transcription family, forms a heterodimer with its cofactor CBF $\beta$  and regulates genes involved in cellular differentiation and progression.<sup>21</sup> RUNX2, also known as osteoblast-specific transcription factor 2 (OSF2), functions as a pivotal participant in osteoblast differentiation and skeletogenesis. Mutations in RUNX2 in humans can cause cleidocranial dysplasia.<sup>22,23</sup> Researchers proved that RUNX2 is a crucial regulator in oncogenic transcriptional programs for various cancers, including GC.<sup>4,24</sup> Zou et al reported that the RUNX2/NID1 axis is responsible for JQ1-mediated inhibition of GC cell proliferation and metastasis.<sup>25</sup> By mining the TCGA and GEO datasets, we showed that the mRNA level of RUNX2 can also predict the outcome of GC patients. Furthermore, RUNX2 significantly promotes the proliferation and increases the self-renewal potential of GC cells. Our previous work proved that the protein level of RUNX2 was significantly correlated with the TNM stage of GC. In this study, we found that RUNX2 was highly expressed in the early stage of GC. These seemingly obscure results suggest that the processes of tumor initiation and tumor progression might share the same modulation model. These results also suggest that RUNX2 is a promising therapeutic target for GC patients.

Accumulating evidence has shown that Hippo signaling pathway activation induces cancer stem cell attributes, proliferation, chemoresistance, and metastasis.<sup>26</sup> YAP1, a crucial transcriptional coactivator in the Hippo signaling pathway, is involved in the initiation and development of several cancers, including GC.<sup>27,28</sup> In 2004, Professor Lian confirmed that the RUNX2-YAP complex is

essential for bone homeostasis, osteoblast activity, and mesenchymal stem cell (MSC) fate determination.<sup>29,30</sup> YAP1 can cooperate with RUNX2 and is crucial for the anchorage-independent growth of cancer cells.<sup>31</sup> Elevated YAP/TAZ expression correlates with the acquisition of malignant CSC features.<sup>15,26</sup> Furthermore, the activation of YAP1 was reported to be a crucial driver of the onset of cervical carcinoma.<sup>32</sup> In GC, elevated YAP expression correlates with a poor outcome and enhances tumor growth.<sup>26</sup> Here, we observed a significant and positive correlation between RUNX2 and YAP1 in GC tissues.

In conclusion, RUNX2 serves as an oncogenic factor that maintains the self-renewal potential of GC cells by positively regulating the YAP signaling pathway. Our observations offer new insights into the molecular mechanisms related to the self-renewal ability of GC cells and provide novel approaches for preventing GC. In addition, RUNX2 could be regarded as a potential biomarker for the detection of early-stage GC and could be a promising novel therapeutic target for late-stage GC patients.

#### ACKNOWLEDGMENT

This study was supported by the National Natural Science Foundation of China (Grants 81972851, 82002448, and 81972793) and the Chongqing Postdoctoral Science Foundation (cstc2019jcyj-bshX0056).

#### CONFLICT OF INTEREST

The authors have no conflicts of interest to declare.

## ORCID

Zhenzhou Yang  <https://orcid.org/0000-0003-2496-1992>

## REFERENCES

1. Siegel RL, Miller KD, Jemal A. Cancer statistics, 2020. *CA Cancer J Clin.* 2020;70:7-30.
2. Van Cutsem E, Sagaert X, Topal B, Haustermans K, Prenen H. Gastric cancer. *Lancet.* 2016;388:2654-2664.
3. Yang L, Ping YF, Yu X, et al. Gastric cancer stem-like cells possess higher capability of invasion and metastasis in association with a mesenchymal transition phenotype. *Cancer Lett.* 2011;310:46-52.
4. Ito Y. RUNX genes in development and cancer: regulation of viral gene expression and the discovery of RUNX family genes. *Adv Cancer Res.* 2008;99:33-76.
5. Guo ZJ, Yang L, Qian F, et al. Transcription factor RUNX2 up-regulates chemokine receptor CXCR4 to promote invasive and metastatic potentials of human gastric cancer. *Oncotarget.* 2016;7:20999-21012.
6. Xia J, Gill EE, Hancock RE. NetworkAnalyst for statistical, visual and network-based meta-analysis of gene expression data. *Nat Protoc.* 2015;10:823-844.
7. Zhou G, Soufan O, Ewald J, Hancock REW, Basu N, Xia J. NetworkAnalyst 3.0: a visual analytics platform for comprehensive gene expression profiling and meta-analysis. *Nucleic Acids Res.* 2019;47:W234-W241.
8. Koch A, De Meyer T, Jeschke J, Van Criekinge W. MEXPRESS: visualizing expression, DNA methylation and clinical TCGA data. *BMC Genom.* 2015;16:636.
9. Gyorffy B, Surowiak P, Budczies J, Lanczky A. Online survival analysis software to assess the prognostic value of biomarkers using transcriptomic data in non-small-cell lung cancer. *PLoS One.* 2013;8:e82241.
10. Szasz AM, Lanczky A, Nagy A, et al. Cross-validation of survival associated biomarkers in gastric cancer using transcriptomic data of 1,065 patients. *Oncotarget.* 2016;7:49322-49333.
11. Wang B, Liu J, Ma LN, et al. Chimeric 5/35 adenovirus-mediated Dickkopf-1 overexpression suppressed tumorigenicity of CD44(+) gastric cancer cells via attenuating Wnt signaling. *J Gastroenterol.* 2013;48:798-808.
12. Liu J, Zhao X, Wang K, et al. A novel YAP1/SLC35B4 regulatory axis contributes to proliferation and progression of gastric carcinoma. *Cell Death Dis.* 2019;10:452.
13. Kawakami R, Mashima T, Kawata N, et al. ALDH1A3-mTOR axis as a therapeutic target for anticancer drug-tolerant persister cells in gastric cancer. *Cancer Sci.* 2020;111:962-973.
14. Dowsett M, Nielsen TO, A'Hern R, et al. Assessment of Ki67 in breast cancer: recommendations from the International Ki67 in Breast Cancer working group. *J Natl Cancer Inst.* 2011;103:1656-1664.
15. Giraud J, Molina-Castro S, Seeneevassen L, et al. Verteporfin targeting YAP1/TAZ-TEAD transcriptional activity inhibits the tumorigenic properties of gastric cancer stem cells. *Int J Cancer.* 2020;146:2255-2267.
16. Breuer K, Foroushani AK, Laird MR, et al. InnateDB: systems biology of innate immunity and beyond—recent updates and continuing curation. *Nucleic Acids Res.* 2013;41:D1228-D1233.
17. Szklarczyk D, Franceschini A, Wyder S, et al. STRING v10: protein-protein interaction networks, integrated over the tree of life. *Nucleic Acids Res.* 2015;43:D447-452.
18. Qin ZY, Wang T, Su S, et al. BRD4 promotes gastric cancer progression and metastasis through acetylation-dependent stabilization of snail. *Cancer Res.* 2019;79:4869-4881.
19. Wang T, Wu H, Liu S, et al. SMYD3 controls a Wnt-responsive epigenetic switch for ASCL2 activation and cancer stem cell maintenance. *Cancer Lett.* 2018;430:11-24.
20. Zhang L, Liu Q, Liu KW, et al. SHARPIN stabilizes beta-catenin through a linear ubiquitination-independent manner to support gastric tumorigenesis. *Gastric Cancer.* 2021;24:402-416.
21. Ichikawa M, Asai T, Saito T, et al. AML-1 is required for megakaryocytic maturation and lymphocytic differentiation, but not for maintenance of hematopoietic stem cells in adult hematopoiesis. *Nat Med.* 2004;10:299-304.
22. Mundlos S, Otto F, Mundlos C, et al. Mutations involving the transcription factor CBFA1 cause cleidocranial dysplasia. *Cell.* 1997;89:773-779.
23. Otto F, Thornell AP, Crompton T, et al. Cbfa1, a candidate gene for cleidocranial dysplasia syndrome, is essential for osteoblast differentiation and bone development. *Cell.* 1997;89:765-771.
24. Onodera Y, Miki Y, Suzuki T, et al. Runx2 in human breast carcinoma: its potential roles in cancer progression. *Cancer Sci.* 2010;101:2670-2675.
25. Zhou S, Zhang S, Wang L, et al. BET protein inhibitor JQ1 downregulates chromatin accessibility and suppresses metastasis of gastric cancer via inactivating RUNX2/NID1 signaling. *Oncogenesis.* 2020;9:33.
26. Zanconato F, Cordenonsi M, Piccolo S. YAP/TAZ at the roots of cancer. *Cancer Cell.* 2016;29:783-803.
27. Ajani JA, Xu Y, Huo L, et al. YAP1 mediates gastric adenocarcinoma peritoneal metastases that are attenuated by YAP1 inhibition. *Gut.* 2021;70(1):55-66.
28. Zhang J, Wong CC, Leung KT, et al. FGF18-FGFR2 signaling triggers the activation of c-Jun-YAP1 axis to promote carcinogenesis in a subgroup of gastric cancer patients and indicates translational potential. *Oncogene.* 2020;39:6647-6663.
29. Zaidi SK, Sullivan AJ, Medina R, et al. Tyrosine phosphorylation controls Runx2-mediated subnuclear targeting of YAP to repress transcription. *EMBO J.* 2004;23:790-799.
30. Han P, Frith JE, Gomez GA, Yap AS, O'Neill GM, Cooper-White JJ. Five piconewtons: the difference between osteogenic and adipogenic fate choice in human mesenchymal stem cells. *ACS Nano.* 2019;13:11129-11143.
31. Vitolo MI, Anglin IE, Mahoney WM Jr, et al. The RUNX2 transcription factor cooperates with the YES-associated protein, YAP65, to promote cell transformation. *Cancer Biol Ther.* 2007;6:856-863.
32. Nishio M, To Y, Maehama T, et al. Endogenous YAP1 activation drives immediate onset of cervical carcinoma in situ in mice. *Cancer Sci.* 2020;111:3576-3587.

## SUPPORTING INFORMATION

Additional supporting information may be found online in the Supporting Information section.

**How to cite this article:** Guo Z, Zhou K, Wang Q, et al. The transcription factor RUNX2 fuels YAP1 signaling and gastric cancer tumorigenesis. *Cancer Sci.* 2021;112:3533-3544. <https://doi.org/10.1111/cas.15045>